

Abstract. Using the sample of radio selected BL Lacertae objects (RBLs) and X-ray selected BL Lacertae objects (XBLs) presented by Sambruna et al. (1996), we calculated the luminosities of radio, optical and X-ray of each source and made the statistical analysis among the luminosities at different wave-bands, broad-band spectral indices from radio to X-ray (α_{rx}) and peak frequencies (ν_p). Our results are as follows: (i) there is a positive correlation between radio luminosity L_r and α_{rx} and a negative correlation between L_r and ν_p . High-energy peak BL Lacs (HBLs) and low-energy peak BL Lacs (LBLs) can be distinguished very well, the dividing lines are probably those of $\log L_r = 43.25$ (erg/sec) and $\alpha_{\text{rx}} > (\text{or } \leq) 0.75$ for $L_r - \alpha_{\text{rx}}$ plot and those of $\log L_r \leq 43.25$ (erg/sec) and $\log \nu_p > 14.7$ for the $L_r - \nu_p$ plot; (ii) there is a weak positive correlation between optical luminosity L_o and α_{rx} and a negatively weak correlation between L_o and ν_p ; (iii) there is no correlation between X-ray luminosity L_X and α_{rx} or between L_X and ν_p . From our analysis, we find that synchrotron radiation is the main X-ray radiation mechanism for HBLs while inverse Compton scattering for LBLs.

Key words: galaxies:BL Lacertae objects:general– galaxies: fundamental parameters:–radiation mechanism: non-thermal

Radio Luminosities and Classificatory Criteria of BL Lacertae Objects

D. C. Mei ^{*}, L. Zhang, Z. J. Jiang, and B. Z. Dai

Department of Physics, Yunnan University, Kunming 650091, P. R. China

Received ; accepted

Most BL Lac objects have been identified in either radio survey (radio-selected BL Lac objects (RBLs) or X-ray survey (X-ray-selected BL Lac objects (XBLs)). These two kinds of BL Lac objects exist many significant differences (for example see, Ledden, O'Dell, 1985; Ghisellini et al. 1986; Stocke et al. 1991). The main differences between RBLs and XBLs are as follows. First, there is a difference in spectral energy distributions (SEDs), RBL-like objects show $\alpha_{\text{rx}} > 0.75$, while XBL-like objects show $\alpha_{\text{rx}} \leq 0.75$ (see, e.g., Ledden, O'Dell, 1985; Stocke et al. 1985; Giommi et al. 1990; Stocke et al. 1991; Schachter et al. 1993; Giommi & Padovani 1994). It should be pointed out that Padovani & Giommi (1995) introduced the distinction between high-energy peak BL Lacs (HBLs) and low-energy peak BL Lacs (LBLs), for objects which emit most of their synchrotron power at high (UV-soft-X) and low (far-IR, optical) frequencies respectively. However, a quantitative distinction can be drawn on the basis of the ratio between radio and X-ray fluxes. It can also use the broad-band spectral index α_{rx} to distinguish HBLs and LBLs: $\alpha_{\text{rx}} \leq 0.75$ for HBLs and $\alpha_{\text{rx}} > 0.75$ for LBLs (Giommi & Padovani 1995). Secondly, there is a difference in the peak frequency distributions (Giommi et al. 1995; Padovani & Giommi, 1995; Urry & Padovani, 1995; Padovani & Giommi, 1996; Lamer et al. 1996). Sambruna et al. (1996) made a parabolic fit to multi-band flux data to obtain the peak frequency of the synchrotron emission, ν_p , of sources, when studying quantitatively how the peak-emission frequency of the synchrotron emission can be used to distinguish RBL-like and XBL-like objects. Making use of the peak frequency, ν_p , of the synchrotron emission estimated by Sambruna et al. (1996). Qin et al. (1999) found that, in the four different regions divided by the $\alpha_{\text{rx}} = 0.75$ line and the $\log \nu_p = 14.7$ line, all RBL-like objects lie in the upper left region, while most XBL-like objects are within the lower right region, with only a few sources being located in the lower left region and no sources being located in

the upper right region. Considering the proper physical origin of the X-ray emission for different classes of BL Lac objects, we calculated the peak frequency ν_p of the synchrotron emission of each source in sample of Sambruna et al. (1996). It was found that all RBL-like objects, defined by $\alpha_{\text{rx}} > 0.75$, are located in the upper-left region, while all XBL-like objects, defined by $\alpha_{\text{rx}} \leq 0.75$, are inside the lower-right region. No sources are in the lower left and upper-right regions, suggesting that the classificatory criteria in terms of the peak frequency should be $\log \nu_p = 14.7$ and the classificatory criteria of the α_{rx} is equal to the classificatory criteria of the $\log \nu_p$ (Dong, Mei, & Liang, 2002). This provides evidence supporting what Giommi et al. (1995) proposed: RBL-like and XBL-like objects can be distinguished by the difference in the peak frequency of the synchrotron emission.

Sambruna et al. (1996) found that the position of the peak frequency $\log \nu_p$ is linked to the luminosity. For more luminous objects, the peak of the synchrotron power locate at lower frequencies. Fossati et al. (1998) studied the spectral energy distributions of three subclass samples of blazars. They also found that despite the differences in continuum shapes for sub-classes of blazars, a unified scheme is possible, blazar continua can be described by luminosity as a fundamental parameter.

In this paper, we will study how the luminosity of each energy band can be used to distinguish RBLs and XBLs. We calculated luminosity of each energy band for RBLs and XBLs presented in Table 1 of Sambruna et al. (1996) in section 2. We present our analysis results in section 3, and give our discussion and conclusions in section 4.

1. Luminosity of BL Lac objects

We calculated the luminosities for the sample of RBLs and XBLs presented by Sambruna et al. (1996). We list the names, red-shifts, broad-band spectral indices, the energy fluxes at radio, optical and X-ray bands and peak frequencies of 23 XBLs in Table 1 and 29 RBLs in Table 2, respectively. Using the logarithmic parabolic form given by Lauda et al (1986) and the data of the energy fluxes

Send offprint requests to: D.C.Mei

* email:kmdcmei@public.km.yn.cn

at radio, optical and X-ray bands, Dong et al. (2002) calculated the peak frequencies of 23 XBLs in Table 1 which are used here. Sambruna et al.(1996) made a parabolic fit to the radio, millimeter, IR, optical, and X-ray fluxes data to obtain the peak frequency, ν_p , of the spectral energy, where, for some XBLs, X-Ray data were not included in the fit. The data of peak frequency ν_p , of the synchrotron emission in Table 2 are made use of Sambruna et al.(1996) except for objects 1652+398 and 2005-489, because the both sources are HBLs ($\alpha_{\text{rx}} < 0.75$). We use the ν_p data of two sources calculated by Dong, Mei & Liang (2002). Therefore, in our sample, there are 27 LBLs which consists of RBLs except for 1652+398 and 2005-489 in Table 2 and 25 HBLs which consists of 23 XBLs and two RBLs (1652+398 and 2005-489).

We calculated rest-frame luminosities of radio, optical and X-ray energy band using the fluxes of BL Lac objects in Table 1 and Table 2. For the K-correction, the flux densities were multiplied by $(1+z)^{\alpha-1}$, where α is the power-law spectral index in the appropriate energy band ($F_\nu \propto \nu^{-\alpha}$). For RBLs, we used $\alpha_r = 0.2$, and $\alpha_{\text{opt}} = 1.05$ (Falomo et al. 1994), while for XBLs we used $\alpha_r = 0$ and $\alpha_{\text{opt}} = 0.65$ (Falomo et al. 1994). We used individual spectral indices in X-ray provided by Sambruna et al.(1996). The redshifts of 0048-097,1147+245 and 1519-273 presented in table 2 of Sambruna et al.(1996) are not available. A mean value of $z = 0.56$ is accordingly adopted for these sources. The flux densities were converted to luminosities using $H_0 = 75 \text{ Km S}^{-1} \text{ Mpc}^{-1}$ and $q_0 = 0.5$, assuming isotropic emission. We calculated the radio luminosity L_r , optical luminosity L_o and X-ray luminosity L_x in rest frame.

2. Results

We now consider the relations among radio luminosity, broad-band spectral index and peak frequency. We plot L_r versus α_{rx} in figure 1a, which shows that the radio luminosity increases as broad-band spectrum index increases. A linear regression analysis yields

$$\log L_r = (6.64 \pm 0.49)\alpha_{\text{rx}} + (38.24 \pm 0.37), \quad (1)$$

where the correlation coefficient is $r = 0.886$ and the chance probability is $p = 2.26 \times 10^{-17}$, $n=52$. Obviously, the correlation is very strong. From this figure, four different regions are divided by the lines $\alpha_{\text{rx}} = 0.75$ and $\log L_r = 43.25$ (ergs^{-1}), all LBLs are located in the upper-right region; all HBLs are inside the lower-left region(two RBLs, 1652+398 and 2005-489 are HBLs); no sources are in the lower-right region and the upper-left region. We plot L_r versus ν_p in figure 1b, which show that the radio luminosity L_r decreases as the peak frequency ν_p increases. The correlation analysis gives

$$\log L_r = -(0.67 \pm 0.06) \log \nu_p + (53.13 \pm 0.92), \quad (2)$$

where the correlation coefficient is $r = -0.841$ and the chance probability is $p = 4.42 \times 10^{-14}$, $n=52$. The correlation is also very strong. In the four different regions

divided by the lines $\nu_p = 14.7$ and $\log L_r = 43.25$, all LBLs are located in the upper-left region; all HBLs are inside the lower-right region(two RBLs, 1652+398 and 2005-489 are HBLs); no sources are in the lower-left region and the upper-right region.

In figure 2, we consider the correlation between the optical luminosity L_o and α_{rx} and that between L_o and ν_p . The results are

$$\log L_o = (2.45 \pm 0.45)\alpha_{\text{rx}} + (43.94 \pm 0.33) \quad (3)$$

with $r = 0.614$ and $p = 2.70 \times 10^{-6}$, $n=52$ and

$$\log L_o = -(0.28 \pm 0.05) \log \nu_p + (49.93 \pm 0.68) \quad (4)$$

with $r = -0.660$ and $p = 2.52 \times 10^{-7}$, $n=52$ respectively. It can be seen that (i)there are a positive correlation between L_o and α_{rx} and a negative correlation between L_o and ν_p , and (ii)HBLs and LBLs can be distinguished by the line of $\alpha_{\text{rx}} \approx 0.75$ (see Fig. 2a) or the line of $\nu_p \approx 14.7$ (see Fig. 2b), but they can not be distinguished by optical luminosity.

Finally, we study the relation of the X-ray luminosity L_x with α_{rx} and ν_p . The correlation analysis reads

$$\log L_x = -(1.41 \pm 0.43)\alpha_{\text{rx}} + (46.08 \pm 0.32) \quad (5)$$

for L_x versus α_{rx} , where $r = -0.42$ and $p = 0.002$.

$$\log L_x = (0.11 \pm 0.05) \log \nu_p + (43.43 \pm 0.73) \quad (6)$$

for L_x versus ν_p , where $r = 0.30$ and $p = 0.03$. Obviously, there is no any correlation between L_x and α_{rx} as well as between L_x and ν_p . We plot the results in Fig. 3. The distributions of HBLs and LBLs in plot of L_x versus α_{rx} (Fig. 3a) and L_x versus ν_p (Fig. 3b) are confusion although the lines of $\alpha_x \approx 0.75$ and $\nu_p \approx 14.7$ can be drawn.

The results of the regression analysis are listed in Table 3.

3. Discussions and conclusions

Sambruna et al.(1996) have made the statistical analysis of the relations of bolometric luminosity L_B (as estimated from parabolic fits to the multi-wavelength from radio to X-ray bands) with position of the peak frequency $\log \nu_p$ and with the broad-band spectral index α_{rx} for the blazars. They found that (i)there is a correlation between L_B and α_{rx} at $> 99\%$ confidence, which may indicate that more luminous objects have steeper α_{rx} , and (ii) more luminous sources have smaller peak frequencies, since the average bolometric luminosity increases from XBLs to RBLs to flat spectrum radio quasars (FSRQs), on average, FSRQs are more luminous and have lower peak frequencies while XBLs are less luminous and have higher peak frequencies. In their analysis, the XBLs and RBLs are not distinguished very well in either L_B - α_{rx} plot or L_B - ν_p plot. In this paper, we have studied the relations of radio, optical and X-ray luminosities with broad-band spectral index (α_{rx}) and peak frequency (ν_p) for 52 BL Lac objects (including 23 XBLs and 29 RBLs). It is different from the analysis of Sambruna et al. (1996), we analyzed the relation of luminosity at the each energy band with α_{rx} and ν_p , respectively.

From our analysis, we found that radio luminosity L_r can be used to distinguish HBLs and LBLs. Our results indicate that there is a very strong positive correlation between L_r and α_{rx} and a negative correlation between L_r and ν_p , more importantly, HBLs and LBLs can be distinguished very well in both L_r - α_{rx} plot (see Fig. 1a) and L_r - ν_p plot (see Fig. 1b). We have also analyzed the relations of the optical and X-ray luminosities with α_{rx} and ν_p , respectively. We found that the optical luminosity has a good correlation with both α_{rx} and ν_p (see Fig. 2a and 2b), but X-ray luminosity shows no any correlation with α_{rx} or ν_p (see Fig. 3a and 3b). Obviously, either L_o or L_x cannot be used to distinguish HBLs and LBLs. Therefore, α_{rx} , ν_p and L_r are equivalent in the classifications of HBLs and LBLs: HBLs fall in the region divided by the lines of $\alpha_{rx} \leq 0.75$ (or $\log \nu_p > 14.7$ Hz) and $\log L_r \leq 43.25$ erg s $^{-1}$ while LBLs in the region divided by the lines of $\alpha_{rx} > 0.75$ (or $\log \nu_p \leq 14.7$ Hz) and $\log L_r > 43.25$ erg s $^{-1}$.

It has been known that the observed spectral energy distributions of BL Lac objects show a peak between IR and X-rays, and the possible radiation mechanism is synchrotron radiation. In Fig. 1a of L_r and α_{rx} plot, HBLs distribute in the region divided by the lines of $\alpha_{rx} \leq 0.75$ and $\log L_r \leq 43.25$ erg s $^{-1}$. Using the definition of α_{rx} and $\alpha_{rx} \leq 0.75$, we have $\log L_x \geq \log L_r + 1$ erg s $^{-1}$ for HBLs where $\nu_r = 5$ GHz and $\nu_x = 1$ keV are used. Since $\log L_r \leq 43.25$ erg s $^{-1}$, we have $\log L_x \geq 44.25$ erg s $^{-1}$ for HBLs while $\log L_x < 44.25$ erg s $^{-1}$ for LBLs. Compared to the result shown in Fig. 3a, the observed X-ray luminosities of HBLs in our sample are above the lower limit of $\log L_x \geq 44.25$ erg s $^{-1}$, indicating that X-rays for HBLs are produced by the synchrotron radiation. From Fig. 3a, the observed X-ray luminosities for most LBLs do not satisfy the upper limit of $L_x < 44.25$ erg s $^{-1}$. We believe that inverse Compton scattering have more important contributions to X-ray emission from these LBLs.

Finally, we would like to point out that we have made the analysis about the relation of energy fluxes at radio, optical and X-ray bands with α_{rx} and ν_p . We find that radio energy flux can be distinguish HBLs and LBLs very well.

Acknowledgements. The Special Funds for Major State Basic Project of China(Grant No.2000077602),the **National 973 project of China (Grant No.NKBRAFG19990754)**, the Natural Science Foundation of China and the Natural Science Foundation of Yunnan province of China are acknowledged for financial support. We would like to thank Dr. J.H.Fan for useful discussion.

References

- Dong, Y. M., Mei, D. C., & Liang, E. W. 2002, PASJ, 54, 171
 Falomo, R., Scarpa, R., & Bersanelli, M. 1994, ApJS, 93, 125
 Fossati, G., et al. 1998, MNRAS, 299, 433
 Ghisellini, G., et al. 1986, ApJ, 310, 317
 Giommi, P., & Padovani, P. 1994, MNRAS, 268, L51
 Giommi, P., Ansari, S. G., & Micol, A. 1995, A&AS, 109, 267.

- Giommi, P., et al. 1990, ApJ, 356, 432
 Lamer, G., Brunner, H., & Staubert, R. 1996, A&A, 311, 384
 Landau, R., et al. 1986, APJ, 308, 78
 Ledden, J. E., & O'Dell, S. L. 1985, ApJ, 298, 630
 Maraschi, L., Ghisellini, G., & Celotti, A. 1992, ApJ, 397, L5
 Padovani, P., & Giommi, P. 1995, ApJ, 444, 567
 Padovani, P., & Giommi, P. 1996, MNRAS, 279, 526
 Qin, Y. P., Xie, G. Z. & Zheng, X. T. 1999, Ap&SS, 266, 549
 Sambruna, R. M., Maraschi, L., & Urry, C. M. 1996, ApJ, 463, 444
 Schachter, J. F., et al. 1993, ApJ, 412, 541
 Stocke, J. T., et al. 1985, ApJ, 298, 619
 Stocke, J. T., et al. 1991, ApJS, 76, 813
 Urry, C. M., & Padovani, P. 1995, PASP, 107, 803

Table 1. Sample of X-ray selected BL lacertae objects (XBLs).

Name	z^*	α_{rx}^*	F_{r}^* (Jy) (5 GHz)	F_{o}^* (mJy) (5500 Å)	F_{x}^* (μ Jy) (1 keV)	$\log \nu_{\text{p}}^{\#}$ (Hz)
0112.1+0903	0.339	0.58	0.0014	0.047 ± 0.001	0.05	15.62
0158.5+0019	0.299	0.51	0.0113	0.21 ± 0.06	1.2	17.34
0205.7+3509	0.318	0.46	0.0036	0.10 ± 0.005	0.90	18.06
0257.9+3429	0.247	0.65	0.010	0.25 ± 0.02	0.10	15.03
0317.0+1834	0.190	0.58	0.017	0.36 ± 0.09	0.54	15.79
0419.3+1943	0.512	0.53	0.008	0.09	0.75	18.31
0607.9+7108	0.267	0.70	0.0182	0.09	0.07	15.23
0737.9+7441	0.315	0.56	0.024	0.64	1.30	16.09
0922.9+7459	0.638	0.55	0.0033	0.044 ± 0.002	0.21	17.21
0950.9+4929	0.207	0.51	0.0033	0.122 ± 0.04	0.27	16.13
1019.0+5139	0.141	0.45	0.0024	0.22	0.93	16.69
1207.9+3945	0.615	0.52	0.0058	0.10	0.55	17.38
1221.8+2452	0.218	0.67	0.0264	0.42 ± 0.09	0.18	15.00
1229.2+6430	0.164	0.56	0.042	0.55 ± 0.17	2.05	16.71
1235.4+6315	0.297	0.55	0.007	0.14 ± 0.02	0.31	16.16
1402.3+0416	0.200	0.57	0.0208	0.88 ± 0.37	0.68	15.39
1407.9+5954	0.495	0.66	0.0165	0.07 ± 0.01	0.10	15.76
1443.5+6349	0.299	0.58	0.0116	0.06	0.35	17.71
1458.8+2249	0.235	0.58	0.0298	1.01 ± 0.20	0.78	15.39
1534.8+0148	0.312	0.61	0.034	0.15 ± 0.05	0.74	17.40
1552.1+2020	0.222	0.54	0.0375	0.44 ± 0.08	2057	17.45
1757.7+7034	0.407	0.50	0.0072	0.18	0.92	17.15
2143.3+0704	0.237	0.61	0.050	0.32 ± 0.04	0.78	16.24

*These data are taken from Tables 1 and 2 of Sambruna et al. (1996).

#These data are taken from Tables 1 of Dong,Mei& Liang (2002).

Table 2. Sample of radio selected BL lacertae objects (RBLs).

Name	z^*	α_{rx}^*	F_r^* (Jy) (5 GHz)	F_o^* (mJy) (5500 Å)	F_x^* (μ Jy) (1 keV)	$\log \nu_p^*$ (Hz)
0048–097	...	0.75	1.110 ± 0.583	2.41 ± 1.63	0.77	13.84
0118–272	>0.557	0.86	1.145 ± 0.075	1.92 ± 0.38	0.20	14.49
0235+164	0.940	0.76	1.81 ± 0.54	1.44 ± 1.06	1.56	13.39
0426–380	>1.030	0.90	1.15 ± 0.03	0.11	0.09	13.22
0454+844	0.112	1.01	1.41 ± 0.14	0.70 ± 0.36	0.02	13.81
0537–441	0.896	0.82	3.93 ± 0.17	1.49 ± 0.43	0.78	14.07
0716+714	>0.300	0.75	0.86 ± 0.18	2.96	1.17	13.79
0735+178	>0.424	0.88	2.13 ± 0.50	3.22 ± 1.56	0.22	14.03
0814+425	0.258	0.98	1.86 ± 0.68	0.26 ± 0.04	0.05	13.34
0851+202	0.306	0.84	2.99 ± 0.56	6.08 ± 5.91	0.70 ± 0.25	13.72
0954+658	0.367	0.88	0.90 ± 0.38	0.86 ± 0.24	0.16	14.09
1144–379	1.048	0.82	1.61 ± 0.96	0.62 ± 0.37	0.41	13.75
1147+245	...	0.92	0.82 ± 0.12	1.53 ± 0.36	0.05	14.58
1308+326	0.997	0.91	2.26 ± 0.40	2.23 ± 1.53	0.13	13.83
1418+546	0.152	0.85	1.22 ± 0.38	2.72 ± 0.82	0.30	13.85
1519–273	...	0.86	2.17 ± 0.25	0.47 ± 0.35	0.39	13.17
1538+149	0.605	0.93	1.53 ± 0.42	0.32 ± 0.10	0.09	13.56
1652+398	0.033	0.67	1.27 ± 0.10	15.65 ± 4.52	8.30	15.01
1749+096	0.320	0.92	1.44 ± 0.36	1.18 ± 0.54	0.14 ± 0.01	13.27
1749+701	0.770	0.81	1.11 ± 0.35	0.99 ± 0.22	0.15	14.43
1803+784	0.679	0.88	2.79 ± 0.30	0.99 ± 0.22	0.26 ± 0.03	13.43
1807+698	0.051	0.87	1.71 ± 0.32	7.85 ± 2.44	0.32	14.26
1823+568	0.664	0.85	1.45 ± 0.21	0.17	0.42	13.65
2005–489	0.071	0.71	1.21 ± 0.02	9.85 ± 1.71	4.12 ± 1.77	14.86
2007+777	0.342	0.91	1.72 ± 0.41	1.17 ± 0.18	0.17	13.66
2131–021	0.557?	0.96	1.84 ± 0.31	0.16 ± 0.04	0.05	13.16
2200+420	0.069	0.85	2.14 ± 0.66	8.65 ± 4.62	0.88	14.25
2240–260	0.774	0.89	1.03	0.26 ± 0.10	0.07	13.32
2254+074	0.190	0.88	0.56 ± 0.27	0.60 ± 0.19	0.09	13.25

*These data are taken from Tables 1 and 2 of Sambruna et al.,(1996).

Table 3. Linear Regression Analysis Results ($y = Ax + B, N = 52$)

y	x	A	B	r	P
$\log L_r$	α_{rx}	6.64 ± 0.49	38.24 ± 0.37	0.886	2.26×10^{-17}
$\log L_r$	ν_p	-0.67 ± 0.06	53.13 ± 0.92	-0.841	4.42×10^{-14}
$\log L_o$	α_{rx}	2.45 ± 0.45	43.94 ± 0.33	0.614	2.70×10^{-6}
$\log L_o$	ν_p	-0.28 ± 0.05	49.93 ± 0.68	-0.660	2.52×10^{-7}
$\log L_x$	α_{rx}	-1.41 ± 0.43	46.08 ± 0.32	-0.42	0.002
$\log L_x$	ν_p	0.11 ± 0.05	43.43 ± 0.73	0.30	0.03

r denotes the correlation coefficient and P denotes the chance probability.

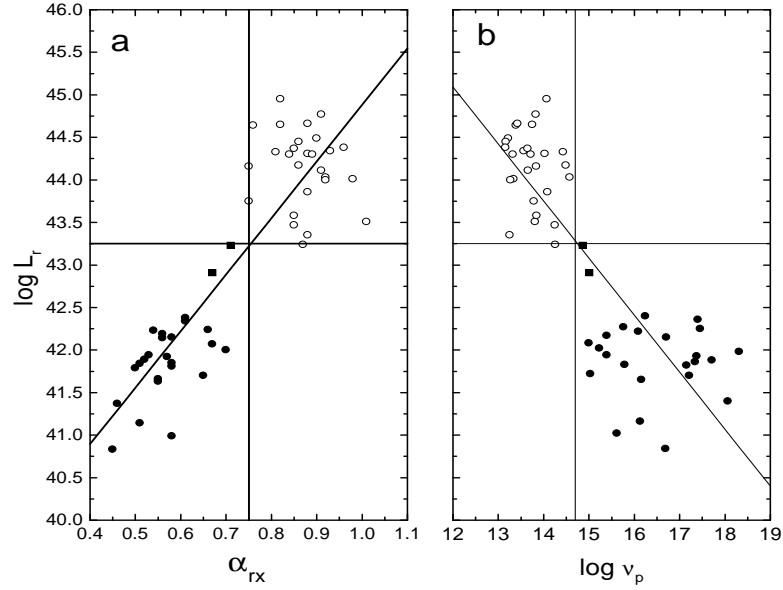


Fig. 1. a: Plot of $\log L_r - \alpha_{rx}$ for RBL and XBL samples. The empty circles represent RBLs, solid squares represent 1652+398 and 2005-489, and the solid circles represent XBLs. The horizontal solid line is $\alpha_{rx} = 0.75$ and the vertical solid line is $\log L_r = 43.25$. The oblique solid line is the regression line $\log L_r = (6.64 \pm 0.49)\alpha_{rx} + (38.24 \pm 0.37)$; b: Plot of $\log L_r - \log \nu_p$ for RBL and XBL samples. The empty circles represent RBLs, solid squares represent 1652+398 and 2005-489, and the solid circles represent XBLs. The horizontal solid line is $\log \nu_p = 14.7$ and the vertical solid line is $\log L_r = 43.25$. The oblique solid line is the regression line $\log L_r = -(0.67 \pm 0.06)\log \nu_p + (53.13 \pm 0.92)$.

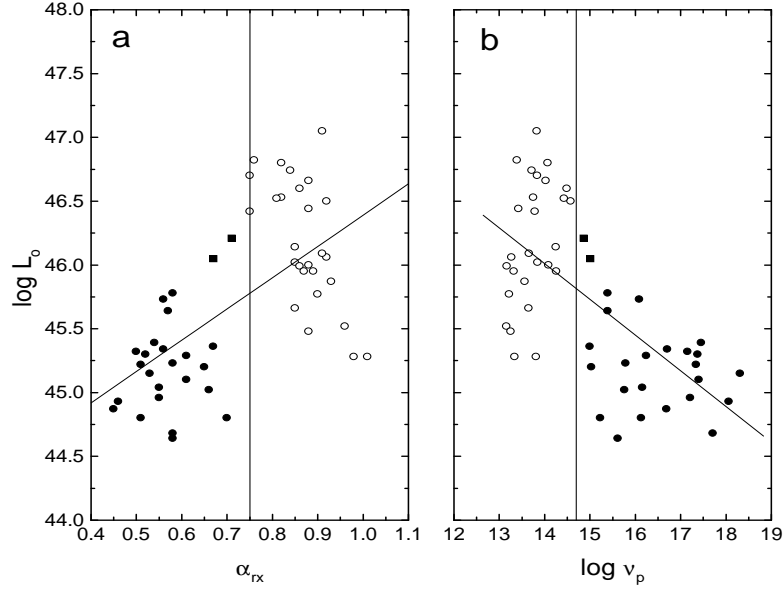


Fig. 2. a: Plot of $\log L_o - \alpha_{rx}$ for RBL and XBL samples. The empty circles represent RBLs, solid squares represent 1652+398 and 2005-489 and the solid circles represent XBLs. The horizontal solid line is $\alpha_{rx} = 0.75$; b: plot of $\log L_o - \log \nu_p$ for RBL and XBL samples. The empty circles represent RBLs, solid squares represent 1652+398 and 2005-489, and the solid circles represent XBLs. The horizontal solid line is $\log \nu_p = 14.7$.

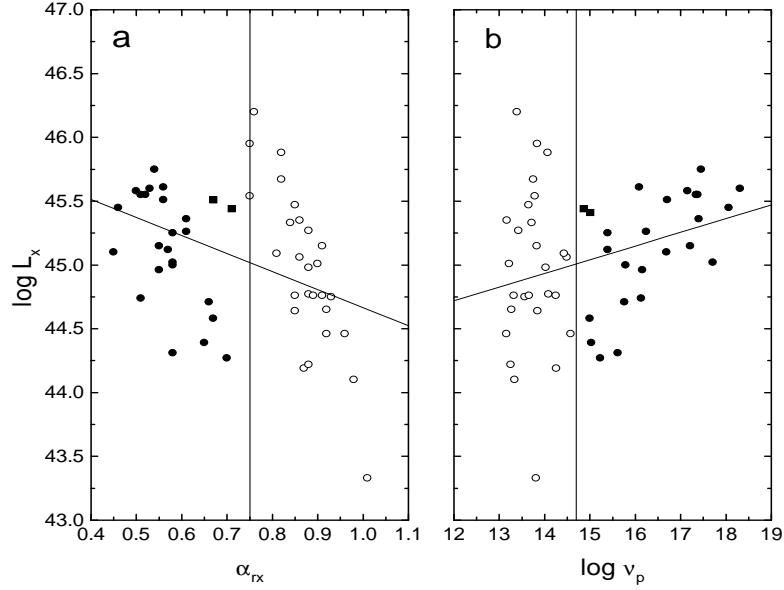


Fig. 3. a: plot of $\log L_x - \alpha_{rx}$ for RBL and XBL samples. The empty circles represent RBLs, solid squares represent 1652+398 and 2005-489 and the solid circles represent XBLs. The horizontal solid line is $\alpha_{rx} = 0.75$; b: plot of $\log L_x - \log \nu_p$ for RBL and XBL samples. The empty circles represent RBLs, solid squares represent 1652+398 and 2005-489, and the solid circles represent XBLs. The horizontal solid line is $\log \nu_p = 14.7$.